Heat conduction in herbertsmithite: Field dependence at the onset of the quantum spin liquid regime

Quentin Barthélemy [1,*] Étienne Lefrançois [1] Jordan Baglo [1] Patrick Bourgeois-Hope,[1] Dipranjan Chatterjee,[2]
Pierre Lefloïc [1] Matias Velázquez,[3] Victor Balédent,[2] Bernard Bernu [4] Nicolas Doiron-Leyraud,[1] Fabrice Bert [2]
Philippe Mendels,[2] and Louis Taillefer [1,5,†]

[1]*Institut Quantique, Département de physique & RQMP, Université de Sherbrooke, Sherbrooke, Québec, Canada J1K 2R1*
[2]*Université Paris-Saclay, CNRS, Laboratoire de Physique des Solides, 91405, Orsay, France*
[3]*Université Grenoble Alpes, CNRS, Grenoble INP, SIMAP, 38000, Grenoble, France*
[4]*Sorbonne Université, CNRS, Laboratoire de Physique Théorique de la Matière Condensée, 75005, Paris, France*
[5]*Canadian Institute for Advanced Research, Toronto, Ontario, Canada M5G 1M1*

We report thermal conductivity measurements on single crystals of herbertsmithite, over a wide range of temperatures (0.05–120 K) in magnetic fields up to 15 T. We also report measurements of the thermal Hall effect, found to be vanishingly small. At high temperatures, in the paramagnetic regime, the thermal conductivity has a negligible field dependence. Upon cooling and the development of correlations, the onset of a clear monotonic field dependence below about 20 K signals a new characteristic temperature scale that may reflect the subtle crossover towards the quantum spin liquid regime. Deconfined spinons, if present, are not detected and phonons, as the main carriers of heat, are strongly scattered by the intrinsic spin excitations and the magnetic defects. In view of the colossal fields required to affect the intrinsic spins, most of the field-induced evolution is attributed to the progressive polarization of some magnetic defects. By elaborating a phenomenological model, we extract the magnetization of these main scattering centers which does not resemble the Brillouin function for free spins $\frac{1}{2}$, requiring to go beyond the paradigm of isolated paramagnetic spins. Besides, the onset of a nonmonotonic field dependence below about 2 K underlines the existence of another characteristic temperature scale, previously highlighted with other measurements, and sheds new light on the phase diagram of herbertsmithite down to the lowest temperatures.

I. INTRODUCTION

The search for a quantum spin liquid (QSL) in two dimensions has been an enduring problem since the resonating valence bond liquid was proposed as a precursor to high-temperature superconductivity in cuprates [1–6]. In theory, it is common to construct QSL states using the projected slave-boson (alternatively slave-fermion) approach for the t-J model at half-filling, assuming the electron is a composite of a spinless bosonic holon and a chargeless spin-$\frac{1}{2}$ fermionic spinon [2–5,7]. Within this spin-charge separation picture, holons and spinons only interact through an emergent U(1) or Z_2 gauge field. As elementary excitations of the QSL, pairs of spinons are formed coherently when pairs of spins are excluded from singlet formation. Deconfined spinons can move away from each other as long as the valence bond liquid can seep between them, through singlet reorganization. In case of hole doping of the QSL, the holon condensation is expected to trigger the conversion of spinon pairs into true Cooper pairs. A central question is therefore the existence of

these mobile fermionic spinons in real two-dimensional QSL candidate materials [8–15].

The mineral herbertsmithite $ZnCu_3(OH)_6Cl_2$ is an emblematic QSL candidate, being one of the best realizations of the nearest-neighbor $S = \frac{1}{2}$ kagome Heisenberg antiferromagnet [16–19]. At the vertices of geometrically perfect kagome planes, magnetic Cu^{2+} ($S = \frac{1}{2}$) ions interact through a strong antiferromagnetic coupling between nearest neighbors $J \sim 190$ K, that far exceeds all other in-plane or interplane couplings [20]. The main perturbations to the pure Heisenberg model consist of (i) the presence of copper ions on about 20% interplane zinc sites, likely producing extended magnetic defects and an effective dilution of the kagome lattice [21–24], and (ii) a finite out-of-plane Dzyaloshinskii-Moriya component $D_z \sim 0.06(2)J$ combined with possible symmetric exchange anisotropy [25–27]. In zero external magnetic field, herbertsmithite does not order or freeze down to the lowest temperatures reached in experiments (20 mK $\sim J/9500$) [17,18] and features a broad continuum of low-energy spin excitations, a characteristic of fractionalization [28,29].

Determining the ground state of the nearest-neighbor $S = \frac{1}{2}$ kagome Heisenberg antiferromagnet remains a major issue for the condensed matter community. As reflected by the massive proliferation of low-lying energy levels in the

*quentin.barthelemy@usherbrooke.ca
†louis.taillefer@usherbrooke.ca

exact spectra of small clusters [30,31], numerical studies point to a collection of very different states with comparable energies including gapped QSL, gapless QSL, or valence bond solids [7,30–51]. Sticking to the fermionic spinon approach, it is now broadly believed that the most relevant candidates are the U(1)[0, π] and Z_2[0, π] (α or β) gapless QSL [7,34,36,39–42,47,48,51]. They feature a spinon band structure with Dirac nodes or small circular Fermi surfaces at the Fermi level (one spinon per site), as opposed to the large Fermi surface proposal for the triangular QSL candidates [52].

Originating from interplane copper ions, magnetic defects which may impact the physics of the kagome planes have been a recurring impediment to probing the pure kagome behavior. In the most straightforward measurements, their contribution is dominant at low temperature and low magnetic field, appearing as a Curie-type tail in susceptibility or Schottky-type term in specific heat [23,24,27,53–55]. Recent specific-heat measurements in high magnetic fields up to 34 T allowed for the first time to separate the QSL behavior of the kagome planes from the Schottky-type anomaly [24]. In a very unexpected way, an effective dilution of the kagome planes had to be introduced while the corresponding specific heat was found to be field independent, from 34 T to zero field, following a power law $C_p^{kago}(T \rightarrow 0) \propto T^\alpha$ with a nontrivial exponent $\alpha \sim 1.5$ in-between the metal-like $\alpha = 1$ (mean-field expectation for a spinon Fermi surface) and the graphenelike $\alpha = 2$ (mean-field expectation for Dirac spinons). This gapless algebraic temperature dependence is typical of a critical QSL but the invariance with field seriously questions the presence of fermionic excitations. In this context, ^{17}O NMR and ^{63,65}Cu NQR appear as ideal probes of the kagome planes and they show the existence of two classes of copper sites: about 60% with a fast relaxation lack a spin excitation gap, in line with the specific-heat results, while 40% display a slow relaxation, the interpretation of which is still debated [23,56–58].

In herbertsmithite, it is also now well established that some field-induced instabilities occur at very low temperatures $T < 2$ K $\sim J/95$, a temperature scale that is most likely determined by the deviations from the pure nearest-neighbor Heisenberg model. From the ^{17}O NMR perspective, the QSL behavior is robust down to at least 1 K ($\sim J/190$) whatever the field intensity up to at least 12 T [59]. At sub-Kelvin temperatures, however, the Gaussian-type line broadens and the spin-lattice relaxation rate drops dramatically along an activation law, which indicates the transition to a random frozen phase with gapped excitations. When constructing a *B-T* phase diagram out of these NMR experiments, the transition between the QSL regime and the frozen phase extrapolates to a possible quantum critical point on the order of 1.55 T in the $T \rightarrow 0$ limit [59]. Such a field-induced transition from a gapless to a gapped regime was similarly reported in the case of Zn-brochantite, another QSL candidate material [60]. Besides, torque magnetometry [61], ac susceptibility [62], and specific-heat [24] measurements revealed an additional (more vertical) in-field crossover extending even slightly above 1 K. Therefore, in order to examine the kagome QSL behavior outside of the energy range in which perturbations have their most severe impact, the focus should be either on measuring herbertsmithite in zero field down to the lowest temperatures or in finite fields at temperatures above 2 K.

In this study, through the prism of thermal transport measurements on herbertsmithite single crystals, we first aim to determine whether the emergent excitations that originate in the field-independent gapless C_p^{kago} give rise to notable spin-mediated heat conduction. Indeed, just as electrons would do in a metal, deconfined spinons may carry heat in addition to phonons, with distinct signatures expected at low temperature depending on the class of the QSL. Recently, Huang *et al.* [63] and Murayama *et al.* [64] have started to explore this issue but concentrated on a small range of very low temperatures (respectively, 0.05–0.8 K and 0.1–0.5 K) in magnetic fields up to 15 T, always away from the QSL regime, within the frozen phase, except in zero field. In both of the aforementioned studies, the authors reported a scarcely field-dependent (if not field-independent) thermal conductivity, the absence of any residual term at $T = 0$, and thus claimed the absence of mobile fermionic excitations (whether gapped or gapless) with the ability to delocalize over large portions of the sample. Nevertheless, the limited set of data calls for the present, more comprehensive study, first to check the results independently and then to investigate potential spinon-phonon decoupling and thermal Hall effect. Extending the measurements to higher temperatures reveals that the thermal conductivity is clearly sensitive to the magnetic field below about 20 K. In our data, the absence of a residual term at $T = 0$, of spinon-phonon decoupling and of thermal Hall effect, even though it does not rule out the presence of deconfined spinons, allow for the rigorous conclusion that phonons are the main carriers of heat. More significant is our observation of two distinct regimes of field dependence, monotonic above about 2 K and nonmonotonic below, which highlight two characteristic low-temperature scales. Our comprehensive study of the field dependence, which we ascribe to a strong phonon scattering from the whole spin ensemble, opens an avenue for characterizing the magnetic defects and helps in clarifying the phase diagram of herbertsmithite down to the lowest temperatures.

II. EXPERIMENTAL DETAILS

We performed thermal conductivity (κ_{xx}) and thermal Hall conductivity (κ_{xy}) measurements on high-quality single crystals of protonated (the PHS sample) and deuterated (the DHS sample) herbertsmithite that were prepared using methods described elsewhere [65,66]. We use the same labels as in Ref. [24] because the samples are obtained in the same way and have similar copper contents. Based on SQUID susceptibility and specific heat data, the DHS sample harbors slightly more magnetic defects than the PHS sample [24]. This is due to the different temperatures used in the growth process. Attributing the Curie-type tail in susceptibility and the Schottky-type term in specific heat to copper ions sitting on the interplane zinc sites leads to an occupation as high as 18% for the PHS sample and 23% for the DHS sample. The samples were measured as grown (uncut) for a wide range of temperatures (0.05–120 K) in magnetic fields up to 15 T, working in variable temperature insert (VTI) and dilution refrigerator (DR) environments with thermocouple and ruthenium oxide temperature sensors, respectively. The samples were first examined with x-ray diffraction to determine the

orientation of the high-symmetry axes. The largest faces, on which the placement of contacts is easier, were not found parallel to the kagome planes contrary to what was assumed in other studies [63,64].

The measurements were carried out by employing a standard steady-state method. A constant heat current **j** is injected at one end of the sample while the other end is thermally sunk to a copper block at bath temperature T_0. The heat current is generated when applying an electrical current through a strain gauge whose resistance marginally depends on the temperature and magnetic field (about 5 kΩ in the VTI and about 10 kΩ in the DR). Assuming a one-dimensional heat flow and an isotropic medium, the longitudinal thermal gradient dT_x is measured between two contacts separated by a distance l along the heat flow. This gradient is evaluated using absolute and differential type-E thermocouples in the VTI, and ruthenium oxide sensors in the DR (calibrated *in situ* against a reference germanium thermometer placed in a field compensated zone). The longitudinal thermal conductivity is then given by $\kappa_{xx} = j/(\alpha dT_x)$ where α is a geometrical factor determined by the cross section wt (w: width, t: thickness) divided by l. In the VTI, in presence of a magnetic field $\mathbf{B} \perp \mathbf{j}$, the transverse thermal gradient dT_y is measured between two contacts separated by the distance w perpendicular to the heat flow. This gradient is evaluated using a differential type-E thermocouple. After antisymmetrization, $dT_y = [dT_y(\mathbf{B}) - dT_y(-\mathbf{B})]/2$, the thermal Hall conductivity is given by $\kappa_{xy} = l\kappa_{yy}dT_y/(wdT_x) = l\kappa_{xx}dT_y/(wdT_x)$.

The contacts consisted of 17-μm gold wires attached with silver paint and had geometries ($l \times w \times t$): $526 \times 774 \times 326$ μm³ for the PHS sample in the DR, $609 \times 293 \times 266$ μm³ for the DHS sample in the DR, and $644 \times 282 \times 334$ μm³ for the (same) DHS sample in the VTI. Uncertainties on the absolute values of κ_{xx}, on the order of 20% at maximum, mainly originate from the uncertainties on the dimensions l, w, and t. The heat current **j** was chosen such that $dT_x/T \sim 5\%$–10% and the resulting κ_{xx} was independent of dT_x/T, indicating no heat loss. Although we made sure that **j** had a large in-plane component j_{ab}, let us recall that the magnetic anisotropy is weak at low temperature [27] and that spinon transport (if any) is expected to occur in all directions, even between the planes [67]. Therefore, the orientations of **j** and **B** do not really matter for this study. We always applied the magnetic field perpendicular to **j** and we did not notice any major difference in terms of shape and magnitude between the data obtained in our three configurations and elsewhere [63,64]. The small mismatch observed in the DHS sample's κ_{xx} between DR and VTI data (enhanced in the semilogarithm display of Fig. 1) mostly arises from the error made when estimating the dimensions l, w, and t.

III. RESULTS

A. From the paramagnetic to the QSL regime

Let us focus first on the data representing the evolution from the high-temperature paramagnetic regime to the QSL regime. We thus rely on the data obtained in zero field at all temperatures and the data obtained in finite fields at temperatures higher than 2 K. These data show a smooth temperature
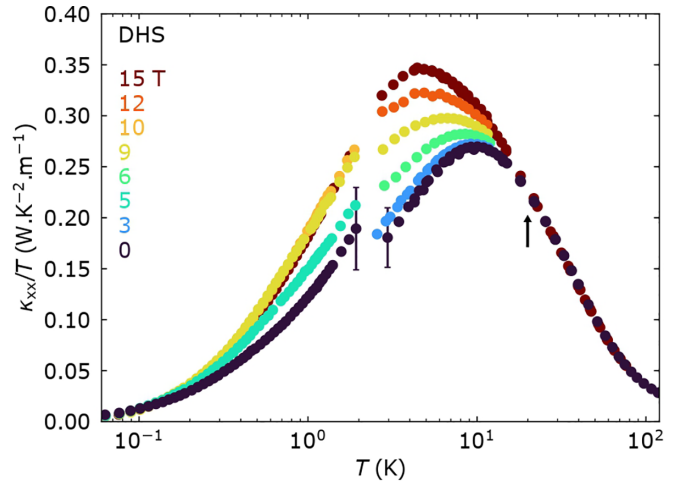
FIG. 1. Thermal conductivity of the DHS sample, as a semilogarithm plot of κ_{xx}/T vs T, for various magnetic fields applied perpendicular to the heat current. Below about 20 K (arrow), κ_{xx} acquires a clear field dependence. We show typical error bars on both sides of the minor discontinuity at about 2 K between the DR and VTI data.

evolution, without any anomaly that could indicate a sharp structural or magnetic transition. A striking feature, however, is the onset of a clear field dependence below about 20 K (see Fig. 1). This observation is a direct rebuttal to recent reports of a scarcely field-dependent (if not field-independent) thermal conductivity, which were based on very-low-temperature data only (below 0.8 K) [63,64]. Here we examine the origin of both the temperature and field dependencies in the QSL regime, investigating the nature of the carriers of heat and their scatterers.

To date, the accumulation of numerical studies on the nearest-neighbor $S = \frac{1}{2}$ kagome Heisenberg antiferromagnet strongly supports the stabilization of a Dirac or small Fermi surface QSL ground state with mobile fermionic spinons [7,34,36,39–42,47,48,51]. In zero field, when embedding some defects, both of these scenarios yield a small but finite density of states at zero temperature [67,69]. In principle, this should result in a residual term in the thermal conductivity [a finite $\kappa_{xx}(T \to 0, B = 0)/T$]. In practice, the accurate detection of such a residual term is challenging and may be prevented by a possible thermal decoupling of spinons from phonons at the lowest temperatures. As it was evidenced with several measurements on some high-T_c cuprates in both the normal and superconducting states, a drop of the heat transfer rate from phonons (the primary heat providers at the hot end of the sample) to electrons (either Fermi sea normal electrons or d-wave Dirac quasiparticles) results in a steep downturn of the thermal conductivity, following $\kappa_{xx}(T \to 0) \propto T^{\eta}$ with η between 4 and 5 [70].

As verified over a large range of temperatures (see Fig. 1), our thermal conductivity data do not show any anomalous downturn so that we can confidently rule out any spinon-phonon decoupling. For both the DHS and PHS samples in zero field, our data can readily be seen to extrapolate to zero as $T \to 0$ (see Fig. 2), in good agreement with recent reports [63,64]. This casts serious doubt on the presence of
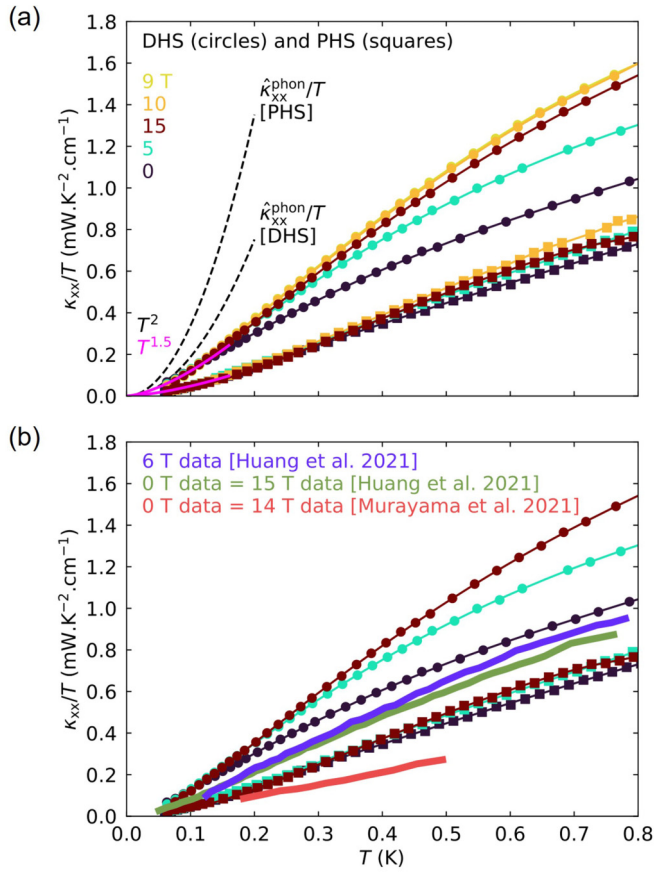
FIG. 2. (a) Thermal conductivity of the two DHS and PHS samples at very low temperatures, as a plot of κ_{xx}/T vs T, for various magnetic fields applied perpendicular to the heat current. Solid lines are a guide to the eye. Below 160 mK and whatever the field intensity, $\kappa_{xx}/T \propto T^{1.5}$ for both samples (extrapolations in pink). Dashed lines depict estimates of $\hat{\kappa}_{xx}^{phon}/T$ in the boundary scattering limit. (b) Some data adapted from Refs. [63,64] (thick lines) are superimposed on our data. The color code is the same in (a) and (b).

deconfined spinons in the ground state of herbertsmithite. Below 0.16 K, for both samples, the best extrapolations correspond to power laws of the form $\kappa_{xx}(T \to 0, B = 0) \propto T^{\eta}$ with $\eta \sim 2.5$.

For temperatures from 10 to 60 K, we also report the absence of any noticeable transverse thermal gradient in the DHS sample when a magnetic field of 15 T (the highest field intensity in our experiments) is applied perpendicular to the heat current. On this range, $|dT_y|$ is found always smaller than 0.5 mK. We cannot rely on measurements at lower temperatures because the thermocouple sensitivity gets significantly degraded and is no longer sufficient to detect such small signals. The "degree of chirality," given by the ratio $|\kappa_{xy}/\kappa_{xx}|$, is much lower than the typical value on the order of 0.1% measured in other insulators for which there is a small but substantial thermal Hall effect, like α-RuCl$_3$ (0.1% at 20 K) or Cu$_3$TeO$_6$ (0.3% at 20 K) (see Fig. 3). This reflects the absence of the large Lorentz-force-driven thermal Hall effect predicted for QSL states with fermionic spinons [71].

Both the lack of spinon-phonon decoupling and sizable thermal Hall effect in the QSL regime were the missing
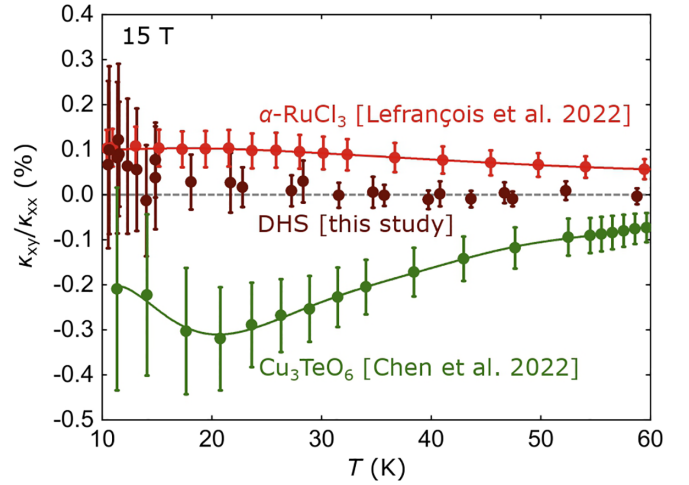
FIG. 3. A plot of the ratio κ_{xy}/κ_{xx} vs T, for the DHS sample, α-RuCl$_3$ (adapted from Ref. [15]) and Cu$_3$TeO$_6$ (adapted from Ref. [68]), in a magnetic field of 15 T applied perpendicular to the heat current. Solid lines are a guide to the eye. For the DHS sample, the ratio κ_{xy}/κ_{xx} remains close to zero (dashed gray line) over a large temperature range 10–60 K.

ts in previous reports to state that there is no evidence of a significant contribution from mobile spin excitations to the heat conduction in herbertsmithite. If the emergent excitations are really mobile, it is then necessary for their mean-free path to be drastically altered, so that they cannot carry the heat efficiently along the entire length of the sample. This would mean that they are either heavily scattered and/or compelled to delocalize over small bounded areas or closed paths like segments or loops. Conservatively, as already suggested by the field-independent specific heat of the kagome planes C_p^{kago}, we suspect that herbertsmithite does not harbor any neutral fermion. Still, thermal conductivity is not the probe to provide a definitive proof for this. It can only tell whether there is a sizable spinon contribution on top of the phonon contribution, and this is not the case here. Hence, in this study, we do not prove the absence of mobile spin excitations, which could ultimately challenge the establishment of a QSL in herbertsmithite, but rather provide evidence that phonons are the main carriers of heat.

Now, if the thermal transport is only ascribed to phonons, we must invoke a strong coupling to the spin degrees of freedom in order to explain the deviation from the expected $\eta = 3$ to the observed $\eta \sim 2.5$ along with the monotonic field dependence. In principle, at very low temperatures, ballistic phonons are primarily scattered by the sample boundaries. In this limit, the thermal conductivity is given by $3\hat{\kappa}_{xx}^{phon} = C_p^{phon} v^{phon} l^{phon}$. $C_p^{phon}(T) = \beta T^3$ is the phonon specific heat, $v^{phon} = (2\pi^2 k_B^4 V_m / 5\beta\hbar^3)^{1/3}$ is the speed of sound where $V_m \simeq 114.3$ cm^3 mol^{-1} is the molar volume of herbertsmithite and $l^{phon} = 2(wt/\pi)^{1/2}$ is the phonon mean-free path set by the sample's width w and thickness t. This mean-free path is about 567 μm for the PHS sample in the DR, 315 μm for the DHS sample in the DR, and about 346 μm for the (same) DHS sample in the VTI. As specific-heat measurements allowed us to determine $\beta = 0.78(3)$ mJ mol^{-1} K^{-4}
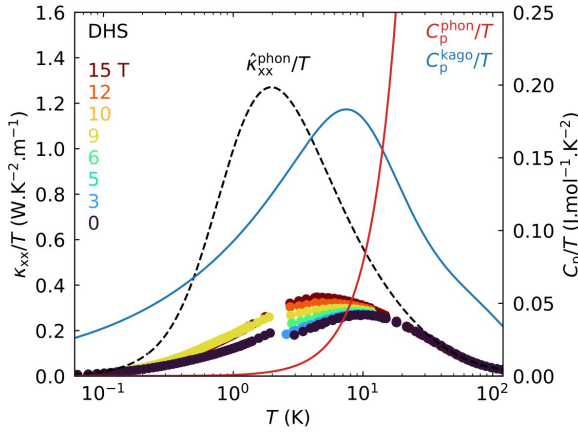
FIG. 4. Left axis: same data as in Fig. 1 and corresponding estimate of $\hat{\kappa}_{xx}^{phon}/T$ over the whole temperature range (dashed line). Right axis: estimate of the phonon specific heat C_p^{phon}/T and computed field-independent specific heat of the kagome planes C_p^{kago}/T (adapted from Ref. [24]).

(the corresponding Debye temperature θ_D is about 151 K) [24] (see Fig. 4), we deduce $v^{phon} \simeq 2620$ m s^{-1} and compute $\hat{\kappa}_{xx}^{phon}$ for each sample (see Fig. 2). Actually, with the use of the Debye-Callaway model, we can even determine the complete evolution of $\hat{\kappa}_{xx}^{phon}$ from room temperature down to the lowest temperatures in the absence of any magnetic scattering, by fitting the defect and umklapp scattering terms on the data above 40 K:

$$\hat{\kappa}_{xx}^{phon}(T) = \frac{k_B^4 T^3}{2\pi^2 \hbar^3 v^{phon}} \int_0^{\theta_D/T} \frac{x^4 e^x}{(e^x - 1)^2} \tau_0(x, T) dx, \quad (1)$$

with $x = h\nu/(k_B T)$ (ν is the phonon frequency) and the non-magnetic scattering rate given by

$$\frac{1}{\tau_0} = \frac{v^{phon}}{l^{phon}} + a\left(\frac{k_B T x}{\hbar}\right)^4 + bT\left(\frac{k_B T x}{\hbar}\right)^2 e^{-\theta_D/3T}, \quad (2)$$

where a and b are the two fit parameters corresponding to the strengths of the defect and umklapp scattering processes [72,73]. In Fig. 4, we plot our best estimate for the DHS sample in the VTI, with $a = 8(2) \times 10^{-41}$ s^3 and $b = 2(1) \times 10^{-18}$ s K^{-1}. We highlight that the measured thermal conductivity is about five times lower at 4 K in zero field. This suggests, as in the case of many other QSL candidates [11,74–76], that phonons are strongly scattered by (i) spin excitations of the quantum paramagnet (whether localized or mobile) and (ii) magnetic defects. Indeed, let us emphasize that C_p^{kago}/T, the Schottky-type anomaly and $\hat{\kappa}_{xx}^{phon}/T$ have a maximum within the same temperature window below 10 K, in a range where the estimate for the phonon specific heat C_p^{phon}/T drops rapidly ($C_p^{phon}/C_p^{kago} \sim 8\%$ at 4 K) [24] (see Fig. 4).

The strong spin phonon coupling is also reflected in the evolution of the thermal conductivity with applied field, namely, the monotonic field dependence which appears below about 20 K down to about 2 K (see Fig. 1). The gradual enhancement of κ_{xx} when increasing the field intensity is then understood in terms of a weakening of the magnetic scattering processes, when some spin fluctuations are suppressed due to the polarization of both the intrinsic spins in the kagome

planes and the magnetic defects. Such a mechanism has already been proposed in the case of the Kondo insulator SmB$_6$, a diluted terbium pyrochlore oxide, and the layered honeycomb magnet CrCl$_3$ for instance [77–80]. Following Ref. [80], we can therefore consider a simple phenomenological model to describe the data, where the ratio $\hat{\kappa}_{xx}^{phon}(T)/\kappa_{xx}(T, B)$ is expressed as $1 + \xi(T, B)$ and the total scattering rate $1/\tau$ is given by the sum of the nonmagnetic scattering rate $1/\tau_0$ and a magnetic scattering rate $1/\tau_m = \xi/\tau_0$. We can write $\xi(T, B)$ as $\lambda^{kago}(T)n^{kago}(T, B) + \lambda^{def}(T)n^{def}(T, B)$ where the field-independent λ parameters represent effective strengths for the spin phonon coupling and the field-dependent n parameters account for the fractions of nonpolarized spins, in both the kagome and magnetic defect systems. We have introduced two separate temperature-dependent couplings because these two systems are characterized by fluctuations with different frequency scales. In zero field, $n^{kago} = n^{def} = 1$ so that $\kappa_{xx}(T, B = 0) = \hat{\kappa}_{xx}^{phon}(T)/[1 + \lambda^{kago}(T) + \lambda^{def}(T)]$. When all the spins are fully polarized, which is never the case even in the strongest magnetic fields available [81], $n^{kago} = n^{def} = 0$ so that $\kappa_{xx}(T)$ reaches $\hat{\kappa}_{xx}^{phon}(T)$. Introducing the reduced magnetizations $m^{kago}(T, B) = 1 - n^{kago}(T, B)$ and $m^{def}(T, B) = 1 - n^{def}(T, B)$, the ratio of scattering rates is rewritten as $-\xi(T, B) = \lambda^{kago}(T)m^{kago}(T, B) + \lambda^{def}(T)m^{def}(T, B) - [\lambda^{kago}(T) + \lambda^{def}(T)]$.

From the data, we extract the field evolution of $-\xi$ at several fixed temperatures between 3 and 10 K so that we can fit λ^{kago}, λ^{def}, and $m^{def}(B)$, for which we use a Hill function with two parameters (u and v): $m^{def}(B) = B^v/(u^v + B^v)$. It turns out to be impossible to fit m^{def} with a Brillouin function, hence the choice of this more generic form. Here, $m^{kago}(T, B)$ is set to an upper bound, based on the analysis presented in the specific-heat study [24]. For the temperatures and fields under scrutiny, it is temperature independent, proportional to the magnetic field, and reaches values only slightly above 5% in 15 T: $m^{kago}(B) \simeq 0.0035B$. The fits are very good with this four-parameter model (λ^{kago}, λ^{def}, u, v) and the deduced temperature evolutions for the two λ couplings reveal that the scattering by magnetic defects becomes dominant below about 8 K (see Fig. 5). Besides, we observe that the deduced Hill functions depicting m^{def} do not resemble the typical Brillouin functions that are routinely used when treating the magnetic defects as nearly free spins $\frac{1}{2}$. They have an initial convex increase (instead of linear) and saturate more slowly (see Fig. 5). Independent of this fit analysis, the same trend is visible in the evolution of $\text{Max}[\kappa_{xx}(T, B) - \kappa_{xx}(T, B = 0)]/\kappa_{xx}(T_{Max}, B = 0)$ as a function of $g\mu_B B/(2k_B T_{Max})$ (taking $g = 2.2$) (see Fig. 6). This key result may help to better understand the nature of some of the magnetic defects, at least those that behave as the main scatterers. Indeed, the m^{def} curves we extract are most likely linear combinations of several magnetization curves, each of them characterizing a specific type of defect that scatters the phonons to a different extent. As λ^{def} is shared, each coefficient in these linear combinations would incorporate a specific defect concentration and coupling renormalization. A complete model, which would account for at least two types of defects as suggested by ESR and NMR studies [23,82], would be overparametrized. Our simple model is not designed to obtain quantitative

(a)

(b)

(c)
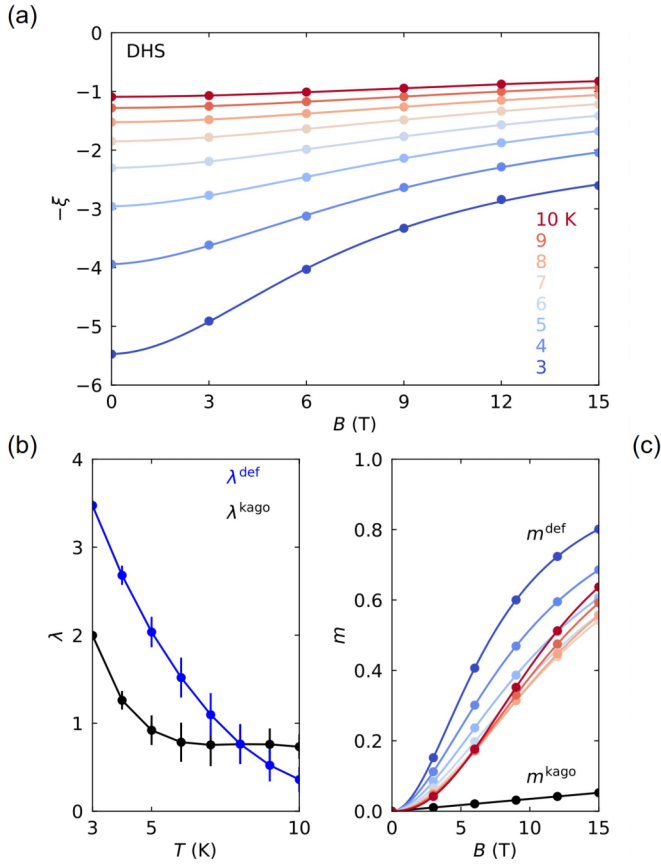
FIG. 5. (a) Field evolution of $-\xi$, extracted for several temperatures between 3 and 10 K. Solid lines are fitted curves (see text). (b) Temperature evolution of the fit parameters λ^{def} and λ^{kago}. (c) Fitted magnetization profiles m^{def} vs B for several temperatures between 3 and 10 K and fixed magnetization profile m^{kago} vs B (based on the results of Ref. [24]). The color scale is the same in (a) and (c).
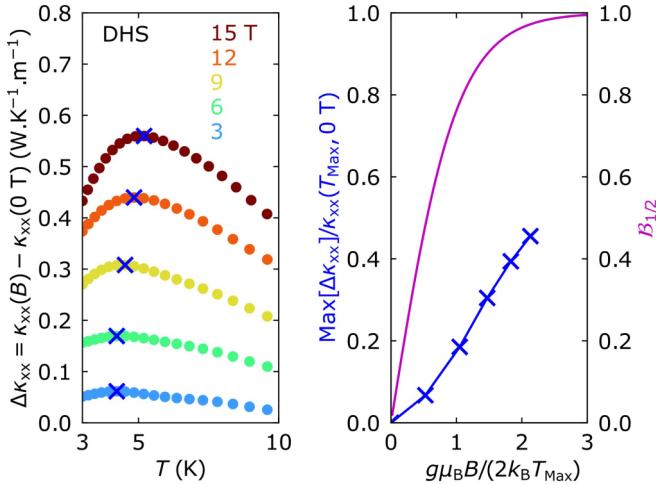
FIG. 6. (a) For the DHS sample, difference between finite-field and zero-field data as a plot of $\Delta\kappa_{\mathrm{xx}} = \kappa_{\mathrm{xx}}(B) - \kappa_{\mathrm{xx}}(0\,\mathrm{T})$ vs T. The maxima positions $[T_{\mathrm{Max}}, \mathrm{Max}(\Delta\kappa_{\mathrm{xx}})]$ are indicated with blue crosses. (b) Left axis (blue): maximal relative increase as a plot of $\mathrm{Max}(\Delta\kappa_{\mathrm{xx}})/\kappa_{\mathrm{xx}}(T_{\mathrm{Max}}, 0\,\mathrm{T})$ vs $g\mu_{\mathrm{B}}B/(2k_{\mathrm{B}}T_{\mathrm{Max}})$, taking $g = 2.2$. Right axis (magenta): normalized magnetization $\mathcal{B}_{1/2}$ of paramagnetic (fully free) spins $\frac{1}{2}$, for comparison. Both trends are not found compatible.

information on m^{def}, although it is already convincing because we note that we retrieve the typical values for the total magnetization when combining about 20% of m^{def} and 80% of m^{kago}, on the order of 15% for $T = 5$ K and $B = 15$ T [83]. Then, while considering the magnitudes and the nonmonotonic temperature evolution of the m^{def} curves (see Fig. 5), we have to keep in mind that m^{kago} may be overestimated and that we do not separate all types of magnetic defects. Our approach is primarily qualitative and the initial convex increase of the m^{def} curves is robust.

B. Very-low-temperature regime ($T < 2$ K)

The field dependence is less prominent at the lowest temperatures (see Fig. 2). In our data, it remains visible down to about 0.13 K and is weaker for the PHS sample than for the DHS sample. It is even weaker in previously reported measurements: it is barely noticeable in the data by Huang *et al.* (0, 3, 6, 12, and 15 T data up to 0.8 K) and invisible in the data by Murayama *et al.* (0 and 14 T data up to 0.5 K) [63,64]. These differences observed from one sample to another are consistent with an essentially extrinsic origin for the field dependence over the whole temperature range, as pointed out in Sec. III A: the DHS sample contains more magnetic defects than the PHS sample. On this basis, the sample used by Huang *et al.* seems to have a slightly lower magnetic defect concentration than the PHS sample. The data by Murayama *et al.* are insufficient to make a guess about the magnetic defect concentration in their sample. Let us stress that the absolute value of the thermal conductivity depends on (i) the uncertainty on the geometrical factors and (ii) the densities of all the scatterers (spin excitations in the kagome planes, structural defects, etc.). In this regard, it is not surprising that the thermal conductivity is higher for the DHS sample (see Fig. 2): if the concentration of magnetic defects is higher, there are fewer spin excitations in the kagome planes to scatter the phonons.

To provide a detailed view of the peculiar field dependence in the very-low-temperature regime, we show some field scans at fixed temperatures obtained for the DHS sample in the DR below 2.22 K [see Fig. 7(a)]. Here, it becomes nonmonotonic below about 1.8 K, which is made very clear when examining the relative variations $[\kappa_{\mathrm{xx}}(B) - \kappa_{\mathrm{xx}}(1.5\,\mathrm{T})]/\kappa_{\mathrm{xx}}(1.5\,\mathrm{T})$ [see Fig. 7(b)]. In this nonmonotonic regime, the thermal conductivity is found to be almost constant up to about 1.5 T, then increases until it reaches a maximal value for fields of about 6–11 T (the maximum seems closer to 6 T in the data by Huang *et al.*) and eventually decreases moderately as the field intensity continues to rise. It seems that a saturation value would be reached if the field intensity was pushed even further.

For temperatures below about 2 K, ^{17}O NMR, torque, susceptibility, inelastic neutron scattering, and specific-heat measurements have already shown the existence of a characteristic temperature scale defining the very-low-temperature regime of herbertsmithite [23,24,29,59,61,62]. This temperature scale is most likely determined by the deviations from the pure nearest-neighbor Heisenberg model (e.g., three-dimensional couplings through interplane magnetic defects and their extensions into the kagome planes,
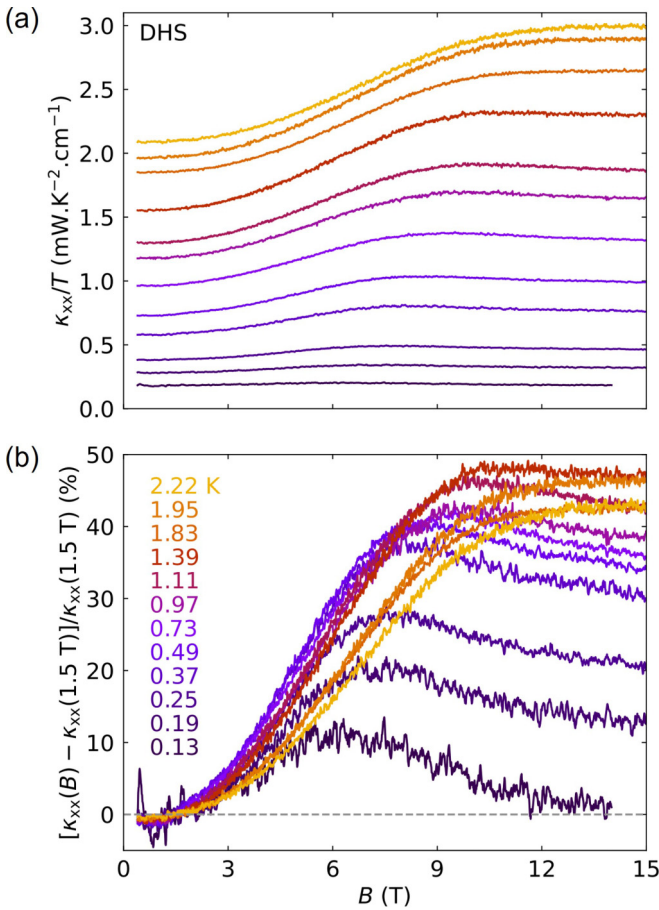
FIG. 7. (a) Thermal conductivity of the DHS sample, as a plot of κ_{xx}/T vs B for various temperatures between 0.13 and 2.22 K. (b) Relative variations as a plot of $[\kappa_{xx}(B) - \kappa_{xx}(1.5\,\mathrm{T})]/\kappa_{xx}(1.5\,\mathrm{T})$ vs B. The color scale is the same in (a) and (b).

Dzyaloshinskii-Moriya interactions, etc.). It features a field-induced transition from the QSL regime to a random frozen phase with gapped excitations and a field-induced crossover of unclear origin [24,59]. The transition occurs for magnetic fields higher than 1.5 T at sub-Kelvin temperatures and is not detected in our experiments. The crossover occurs for magnetic fields higher than 10 T and seems to correspond to the inflection point of $[\kappa_{xx}(B) - \kappa_{xx}(1.5\,\mathrm{T})]/\kappa_{xx}(1.5\,\mathrm{T})$ at high fields, before saturation.

The initial increase of $[\kappa_{xx}(B) - \kappa_{xx}(1.5\,\mathrm{T})]/\kappa_{xx}(1.5\,\mathrm{T})$ for fields up to 6–11 T is observed whatever the temperature below 2.22 K and indicates that the spins are progressively polarized, whether we are referring to two decoupled spin systems in the QSL regime (the magnetic defects and the intrinsic spins in the kagome planes) or the whole ensemble of frozen spins in the glassy regime at the lowest temperatures. Below about 1.8 K, the decrease of the thermal conductivity at higher fields (namely, the appearance of nonmonotonic field dependence) reveals that new scatterers appear. It is then natural to think of spin excitations resulting from a partially polarized state, like ferromagnetic magnons, to scatter the phonons. These spin excitations are expected to vanish at sufficiently high fields so that the phonon thermal conductivity should level off at the value given by $\hat{\kappa}_{xx}^{phon}$ and then reach

the boundary scattering limit at the lowest temperatures. Yet, down to 0.13 K, field scans extrapolate to lower values than $\hat{\kappa}_{xx}^{phon}$ at high fields, suggesting that a substantial amount of spin excitations remain active.

IV. DISCUSSION

A. Phonons as the main carriers of heat

To summarize, with the absence of a residual linear term in the $T \to 0$ limit in zero field, of visible decoupling at low temperatures and of a sizable thermal Hall effect, we have shown that there is no clear sign pointing to a direct contribution from neutral fermions to the thermal conductivity. Phonons remain the main carriers of heat from the highest down to the lowest temperatures. This does not mean that the emergent spin excitations are immobile, as they may simply be constrained to delocalize over limited portions of the sample. Still, the absence of spin-mediated thermal transport calls into question the class of the ground state. In particular, one must ask whether the seemingly local character of the emergent spin excitations is an intrinsic property of the pure Heinsenberg model or rather a consequence of perturbations such as magnetic defects.

On the theory side, it seems now necessary to test the robustness of the leading QSL proposals to the presence of magnetic defects and determine how the mobility of the spinons is impacted. Various studies already focused on the local response (which may be screened by a spinon Kondo effect [84,85]) expected around vacancies and spinless or spinful defects in several types of QSL ground states [86–89], but did not really examine how the full QSL response is modified for a modest defect concentration as in the case of herbertsmithite. Only the case of a large defect concentration inducing a severe quenched bond randomness was treated and found to result in the stabilization of a gapless valence bond glass made of random singlets [90–92]. Adapting this scenario to the case of herbertsmithite requires an unrealistic distribution of couplings $\Delta J/J$ on the order of 0.4 [91]. The upper bound set by ^{17}O NMR is at least an order of magnitude smaller [23].

For some time now, the $Z_2[0, \pi]$ (α or β) and parent $U(1)[0, \pi]$ gapless QSL have been regularly proposed as leading candidates for the ground state of the pure Heisenberg model [7,34,36,39–42,47,48,51]. They are constructed from the slave-boson approach and involve spinons with a nodal or very small circular Fermi surface. The field-independent specific heat C_p^{kago} tends to rule them out in herbertsmithite, as we expect a field-induced response in presence of weakly interacting fermionic excitations. Let us emphasize, however, that the spinons are not completely free to move even when deconfined. In particular, the mean field ansatz of a Z_2 QSL, similar to the Bogoliubov–de Gennes Hamiltonian of a superconductor, includes a spinon pairing term [7]. This term, as it further complexifies the interactions between spinons on the lattice, leads to fascinating properties and may help to explain the lack of a significant spinon contribution to the thermal conductivity, as well as other experimental results. First, very much like Cooper pairs in a superconductor, it is possible that spinon pairs do not carry entropy and thus

heat. Second, the nearest-neighbor spin correlations become anisotropic so that the establishment of the QSL breaks some lattice symmetries, causing the unpaired spinons to move only along the directions of the most correlated bonds [39]. In this vein, ESR, optical ellipsometry, and wavelength-dependent multiharmonic optical polarimetry studies revealed a subtle monoclinic distortion in herbertsmithite, that appears to grow with the building up of short-range correlations [82,93]. If this slight structural change is really driven by the formation of the QSL, it is then very likely that the spinons in herbertsmithite move in specific directions. The most correlated bonds do not necessarily form connected paths, especially if several domains nucleate or if some magnetic defects split some segments of the paths. Such a scenario would naturally account for the lack of spin-mediated thermal transport.

B. New characteristic temperature scale

The temperature of about 20 K below which the thermal conductivity becomes clearly field dependent and deviates from the Debye-Callaway limit in the absence of any magnetic scattering ($\hat{\kappa}_{xx}^{\text{phon}}$) appears to be a new characteristic temperature for herbertsmithite. In the QSL regime, we attributed the small amplitude and the monotonic field dependence of the thermal conductivity to a strong scattering of phonons from emergent excitations of the QSL and from magnetic defects. The occurrence of these two scattering processes seems simultaneous at all fields and points to the establishment of the QSL regime. Indeed, as long as the temperature is high enough to keep all the spins in a conventional paramagnetic regime, the spins that will be eventually involved in the magnetic defects and in the QSL regime at lower temperatures remain indistinguishable. The magnetic defects appear only when the QSL settles, entangling some spins and excluding others.

In fact, we notice that this temperature of about 20 K coincides with the temperature at which multiple contributions (one "main" and two "defect" sets of five peaks) begin to clearly appear in the ^{17}O NMR spectra [23]. Correspondingly, the spin-lattice relaxation rate determined with ^{17}O NMR and Cu NQR starts to combine a fast component and a slow component [23,57]. However, it does not seem suitable to connect this temperature with other special temperatures already identified in herbertsmithite. First, torque measurements revealed that a change of magnetization easy axis occurs at lower temperatures on the order of 12 K [82]. Indeed, below this threshold, the susceptibility of the magnetic defects considerably exceeds the susceptibility of the spins involved in the QSL regime. There is no reason for this change of anisotropy to yield the onset of the field dependence and we further note that our data do not present any anomaly in the relevant temperature range to signal this behavior. Second, NMR measurements showed that the ^{35}Cl spin-lattice relaxation rate peaks at much higher temperatures on the order of 50 K, simultaneously with a sudden change of the ^{17}O quadrupolar frequency at some defect sites [56,94,95]. This was attributed to the freezing of some OH bonds with random orientations. Again, there is no clue for this subtle structural transition in our data, nor obvious relation with the onset of field dependence.

Then, thanks to the strong spin-lattice coupling in herbertsmithite, it appears that thermal transport is a tool of choice to detect the subtle crossover towards the QSL regime. At the end, magnetic defects are both problematic and useful. On the one hand, the QSL class cannot be properly characterized as soon as a substantial amount of magnetic defects is likely to affect the mobility of the emergent excitations: fully localized spin excitations or barely mobile spin excitations lead to the same absence of spin-mediated heat transport. On the other hand, the onset of field dependence combined with the appearance of two magnetic scattering processes implies that magnetic defects have nucleated on top of a new underlying state which encompasses all other spins. In this regard, magnetic defects help to reveal the establishment of the QSL. These observations call for complementary measurements on other QSL candidate materials for which we could vary the concentration of magnetic defects, as in the Zn-brochantite, Zn-barlowite, Zn-claringbullite, and Zn-averievite families by adjusting the zinc content.

C. Negligible phonon Hall effect

We did not detect any sizable thermal Hall effect in herbertsmithite. On the one hand, this is an indication that the spin excitations, if mobile, are bad heat carriers with respect to phonons. Indeed, deconfined spinons that delocalize with a large mean-free path should give rise to a significant Lorentz force driven thermal Hall effect, which is expected to scale with their direct contribution to the longitudinal conductivity (null here) [71]. On the other hand, it is clear that there is no sign of a phonon thermal Hall effect either. We put these observations in perspective with results obtained on other insulators.

Four frustrated magnets with a kagome geometry have already been studied through thermal Hall effect measurements, namely, Cu$(1 - 3,$bdc), volborthite, Ca-kapellasite and Cd-kapellasite [9,10,13,96]. In practice, these materials have fewer magnetic defects than herbertsmithite but involve competing anisotropic interactions, resulting in very different magnetic models. Unlike herbertsmithite, they eventually order at low temperature. In all four cases, there is evidence that some mobile spin excitations contribute to the heat conduction along with the phonons and generate a sizable thermal Hall effect: magnons in Cu$(1 - 3,$bdc) and bosonic spinons in volborthite, Ca-kapellasite, and Cd-kapellasite. In particular, the thermal Hall effect of volborthite, Ca-kapellasite, and Cd-kapellasite is very well captured by the Schwinger-boson mean-field theory from the slave-fermion approach.

There are other evidences for a thermal Hall effect from mobile spin excitations in various nonkagome materials. Actually, the first magnon thermal Hall effect was observed in the pyrochlore ferromagnet Lu$_2$V$_2$O$_7$ [97]. Later on, the thermal Hall effect detected in the quantum spin-ice pyrochlore Tb$_2$Ti$_2$O$_7$ was assigned to more exotic spin excitations [98]. More recently, the Kitaev spin liquid candidate α-RuCl$_3$ came under the spotlight with several conflicting measurements of a thermal Hall effect, either half-quantized and ascribed to Majorana fermions, or not quantized and ascribed to bosonic edge excitations such as topological magnons [99–101].

It is now established that phonons can also generate a thermal Hall effect, whether in presence or absence of magnetic ions. This effect was first observed in 2005 in the paramagnetic garnet $Tb_3Ga_5O_{12}$ [102,103]. More recently, it was observed in a wide variety of systems, often with an unexpectedly large magnitude: the multiferroic ferrimagnetic $Fe_2Mo_3O_8$ [104], some cuprates [105–107], the quantum paraelectric $SrTiO_3$ [108], the cubic antiferromagnet Cu_3TeO_6 [68], the kagome antiferromagnet Cd-kapellasite [13], and the Kitaev QSL candidate α-$RuCl_3$ [15]. Yet, the phonons are not chiral particles and, despite growing theoretical developments on that matter, the reasons why they can be preferentially deflected in one direction or the other depending on the sign of the applied magnetic field still remain enigmatic.

Among the proposed scenarios, there are some intrinsic mechanisms, where the vibrational modes strongly couple to the ionic environment and its defining electric and magnetic moments. These moments shall interact with the applied magnetic field, sometimes in a very subtle way only, and this may eventually give rise to a detectable time-reversal odd contribution to the Berry curvature of phonons [109]. We emphasize that intrinsinc mechanisms are generally predicted to result in a small amplitude, that would become significant under very special circumstances only. In the case of $SrTiO_3$, for instance, an intrinsic effect may arise due to the flexoelectric coupling of phonons to their nearly ferroelectric environment, but is predicted to be orders of magnitude smaller than the actual observation [108,110]. However, if they do not average to zero because of domains, some intrinsic mechanisms could be argued in the case of $Fe_2Mo_3O_8$, and possibly the cases of Cd-kapellasite and α-$RuCl_3$, where a strong spin-lattice coupling may prevail [104,111].

There are also some extrinsic mechanisms, where time-reversal oddness may originate from skew scattering and side jump from defects [112–115]. Extrinsic mechanisms are generally predicted to result in a larger magnitude and have been invoked to explain the observations on $Tb_3Ga_5O_{12}$ and $SrTiO_3$. In $Tb_3Ga_5O_{12}$, the phonon Hall effect is attributed to a resonant scattering from the crystal-field states of super-stoichiometric Tb^{3+} defects [116]. In $SrTiO_3$, it is attributed to a scattering from twin boundaries between tetragonal domains [108,110].

In principle, herbertsmithite has both the intrinsic and extrinsic ingredients to enable the generation of a phonon Hall effect, namely, a strong spin-lattice coupling and a substantial number of extrinsic scatterers. Yet, the observed signal is vanishingly small in both the paramagnetic and QSL regimes, albeit the magnitude of the longitudinal thermal conductivity is higher than that detected in α-$RuCl_3$ and Cd-kapellasite [13,15]. It underlines that the phonon Hall effect occurs in a magnetic insulator only when specific requirements are met for (i) the nature of the intrinsic magnetic state (ordered or disordered, frozen or dynamical) and (ii) the type of the defects (magnetic or nonmagnetic), so that the spin textures developing around the defects drive the phonons in a preferred direction depending on the sign of the magnetic field.

V. CONCLUSION

We have measured the thermal conductivity and thermal Hall conductivity of herbertsmithite. Given the absence of a residual linear term in the $T \to 0$ limit in zero field, of visible decoupling at low temperatures and of a sizable thermal Hall effect, we conclude that deconfined spinons, if present, are not contributing significantly to the heat conduction in the QSL regime. Phonons are found to be the main carriers of heat down to the lowest temperatures. Our data reveal that the thermal conductivity, which is field independent at high temperatures, acquires a clear field dependence below about 20 K, monotonic above about 2 K and nonmonotonic below. The onset of the monotonic field dependence is mainly ascribed to the polarization of some magnetic defects and is thought to signal the establishment of the QSL regime. By extracting the magnetization profile of some of the magnetic defects, we show that they are not isolated paramagnetic objects. This calls for further investigations to understand their spatial extension and their impact on the kagome planes. The nonmonotonic field dependence is found compatible with previously reported instabilities at very low temperatures and suggests that magnetic fields larger than 15 T are required to fully polarize the field-induced glassy phase.

Note added. Recently, it came to our attention that Murayama *et al.* have supplemented their data [117]. Still restricted to magnetic fields of 0 and 14 T, their data now range from 0.1 to 5 K (0.1 to 0.5 K before [64]). In contrast to our findings, they report an identical thermal conductivity for both fields, up to 5 K, and conclude that the spin-phonon coupling is vanishingly small.

[1] P. W. Anderson, The resonating valence bond state in La_2CuO_4 and superconductivity, Science **235**, 1196 (1987).

[2] G. Baskaran, Z. Zou, and P. W. Anderson, The resonating valence bond state and high-T_c superconductivity - a mean field theory, Solid State Commun. **63**, 973 (1987).

[3] X.-G. Wen, Quantum orders and symmetric spin liquids, Phys. Rev. B **65**, 165113 (2002).

[4] P. A. Lee, N. Nagaosa, and X.-G. Wen, Doping a Mott insulator: Physics of high-temperature superconductivity, Rev. Mod. Phys. **78**, 17 (2006).

[5] L. Savary and L. Balents, Quantum spin liquids: A review, Rep. Prog. Phys. **80**, 016502 (2017).

[6] C. Broholm, R. J. Cava, S. A. Kivelson, D. G. Nocera, M. R. Norman, and T. Senthil, Quantum spin liquids, Science **367**, eaay0668 (2020).

[7] Y.-M. Lu, G. Y. Cho, and A. Vishwanath, Unification of bosonic and fermionic theories of spin liquids on the kagome lattice, Phys. Rev. B **96**, 205150 (2017).

[8] M. Yamashita, N. Nakata, Y. Senshu, M. Nagata, H. M. Yamamoto, R. Kato, T. Shibauchi, and Y. Matsuda, Highly mobile gapless excitations in a two-dimensional candidate quantum spin liquid, Science **328**, 1246 (2010).

[9] D. Watanabe, K. Sugii, M. Shimozawa, Y. Suzuki, T. Yajima, H. Ishikawa, Z. Hiroi, T. Shibauchi, Y. Matsuda, and M. Yamashita, Emergence of nontrivial magnetic excitations in a spin-liquid state of kagomé volborthite, Proc. Natl. Acad. Sci. USA **113**, 8653 (2016).

[10] H. Doki, M. Akazawa, H.-Y. Lee, J. H. Han, K. Sugii, M. Shimozawa, N. Kawashima, M. Oda, H. Yoshida, and M. Yamashita, Spin Thermal Hall Conductivity of a Kagome Antiferromagnet, Phys. Rev. Lett. **121**, 097203 (2018).

[11] P. Bourgeois-Hope, F. Laliberté, E. Lefrançois, G. Grissonnanche, S. R. de Cotret, R. Gordon, S. Kitou, H. Sawa, H. Cui, R. Kato, L. Taillefer, and N. Doiron-Leyraud, Thermal Conductivity of the Quantum Spin Liquid Candidate EtMe$_3$ Sb[Pd(dmit)$_2$]$_2$: No Evidence of Mobile Gapless Excitations, Phys. Rev. X **9**, 041051 (2019).

[12] J. M. Ni, B. L. Pan, B. Q. Song, Y. Y. Huang, J. Y. Zeng, Y. J. Yu, E. J. Cheng, L. S. Wang, D. Z. Dai, R. Kato, and S. Y. Li, Absence of Magnetic Thermal Conductivity in the Quantum Spin Liquid Candidate EtMe$_3$ Sb[Pd(dmit)$_2$]$_2$, Phys. Rev. Lett. **123**, 247204 (2019).

[13] M. Akazawa, M. Shimozawa, S. Kittaka, T. Sakakibara, R. Okuma, Z. Hiroi, H.-Y. Lee, N. Kawashima, J. H. Han, and M. Yamashita, Thermal Hall Effects of Spins and Phonons in Kagome Antiferromagnet Cd-Kapellasite, Phys. Rev. X **10**, 041059 (2020).

[14] N. Li, Q. Huang, X. Y. Yue, W. J. Chu, Q. Chen, E. S. Choi, X. Zhao, H. D. Zhou, and X. F. Sun, Possible itinerant excitations and quantum spin state transitions in the effective spin-1/2 triangular-lattice antiferromagnet Na$_2$BaCo(PO$_4$)$_2$, Nat. Commun. **11**, 4216 (2020).

[15] É. Lefrançois, G. Grissonnanche, J. Baglo, P. Lampen-Kelley, J.-Q. Yan, C. Balz, D. Mandrus, S. E. Nagler, S. Kim, Y.-J. Kim, N. Doiron-Leyraud, and L. Taillefer, Evidence of a Phonon Hall Effect in the Kitaev Spin Liquid Candidate α-RuCl$_3$, Phys. Rev. X **12**, 021025 (2022).

[16] M. P. Shores, E. A. Nytko, B. M. Bartlett, and D. G. Nocera, A Structurally perfect $S = 1/2$ kagome antiferromagnet, J. Am. Chem. Soc. **127**, 13462 (2005).

[17] P. Mendels, F. Bert, M. A. de Vries, A. Olariu, A. Harrison, F. Duc, J. C. Trombe, J. S. Lord, A. Amato, and C. Baines, Quantum Magnetism in the Paratacamite Family: Towards an Ideal Kagomé Lattice, Phys. Rev. Lett. **98**, 077204 (2007).

[18] P. Mendels and F. Bert, Quantum kagome frustrated antiferromagnets: One route to quantum spin liquids, C. R. Phys. **17**, 455 (2016).

[19] M. R. Norman, Colloquium: Herbertsmithite and the search for the quantum spin liquid, Rev. Mod. Phys. **88**, 041002 (2016).

[20] H. O. Jeschke, F. Salvat-Pujol, and R. Valenti, First-principles determination of Heisenberg Hamiltonian parameters for the spin-$\frac{1}{2}$ Kagome Antiferromagnet ZnCu$_3$(OH)$_6$Cl$_2$, Phys. Rev. B **88**, 075106 (2013).

[21] D. E. Freedman, T.-H. Han, A. Prodi, P. Müller, Q.-Z. Huang, Y.-S. Chen, S. M. Webb, Y. S. Lee, T. M. McQueen, and D. G. Nocera, Site specific X-ray anomalous dispersion of the geometrically frustrated kagomé magnet, herbertsmithite, ZnCu$_3$(OH)$_6$Cl$_2$, J. Am. Chem. Soc. **132**, 16185 (2010).

[22] R. W. Smaha, I. Boukahil, C. J. Titus, J. M. Jiang, J. P. Sheckelton, W. He, J. Wen, J. Vinson, S. G. Wang, Y.-S. Chen, S. J. Teat, T. P. Devereaux, C. D. Pemmaraju, and Y. S. Lee, Site-specific structure at multiple length scales in kagome quantum spin liquid candidates, Phys. Rev. Mater. **4**, 124406 (2020).

[23] P. Khuntia, M. Velázquez, Q. Barthélemy, F. Bert, E. Kermarrec, A. Legros, B. Bernu, L. Messio, A. Zorko, and P. Mendels, Gapless ground state in the archetypal quantum kagome antiferromagnet ZnCu$_3$(OH)$_6$Cl$_2$, Nat. Phys. **16**, 469 (2020).

[24] Q. Barthélemy, A. Demuer, C. Marcenat, T. Klein, B. Bernu, L. Messio, M. Velázquez, E. Kermarrec, F. Bert, and P. Mendels, Specific Heat of the Kagome Antiferromagnet Herbertsmithite in High Magnetic Fields, Phys. Rev. X **12**, 011014 (2022).

[25] A. Zorko, S. Nellutla, J. van Tol, L. C. Brunel, F. Bert, F. Duc, J. C. Trombe, M. A. de Vries, A. Harrison, and P. Mendels, Dzyaloshinsky-Moriya Anisotropy in the Spin-1/2 Kagome Compound ZnCu$_3$(OH)$_6$Cl$_2$, Phys. Rev. Lett. **101**, 026405 (2008).

[26] S. El Shawish, O. Cepas, and S. Miyashita, Electron spin resonance in $S = \frac{1}{2}$ antiferromagnets at high temperature, Phys. Rev. B **81**, 224421 (2010).

[27] T.-H. Han, S. Chu, and Y. S. Lee, Refining the Spin Hamiltonian in the Spin-$\frac{1}{2}$ Kagome Lattice Antiferromagnet ZnCu$_3$(OH)$_6$Cl$_2$ Using Single Crystals, Phys. Rev. Lett. **108**, 157202 (2012).

[28] T.-H. Han, J. S. Helton, S. Chu, D. G. Nocera, J. A. Rodriguez-Rivera, C. Broholm, and Y. S. Lee, Fractionalized excitations in the spin-liquid state of a kagome-lattice antiferromagnet, Nature (London) **492**, 406 (2012).

[29] T.-H. Han, M. R. Norman, J.-J. Wen, J. A. Rodriguez-Rivera, J. S. Helton, C. Broholm, and Y. S. Lee, Correlated impurities and intrinsic spin-liquid physics in the kagome material herbertsmithite, Phys. Rev. B **94**, 060409(R) (2016).

[30] P. Lecheminant, B. Bernu, C. Lhuillier, L. Pierre, and P. Sindzingre, Order versus disorder in the quantum Heisenberg antiferromagnet on the kagomé lattice using exact spectra analysis, Phys. Rev. B **56**, 2521 (1997).

[31] P. Sindzingre and C. Lhuillier, Low-energy excitations of the kagomé antiferromagnet and the spin-gap issue, Europhys. Lett. **88**, 27009 (2009).

[32] S. Sachdev, Kagomé- and triangular-lattice Heisenberg antiferromagnets: Ordering from quantum fluctuations and

quantum-disordered ground states with unconfined bosonic spinons, Phys. Rev. B **45**, 12377 (1992).

[33] C. Waldtmann, H.-U. Everts, B. Bernu, C. Lhuillier, P. Sindzingre, P. Lecheminant, and L. Pierre, First excitations of the spin 1/2 Heisenberg antiferromagnet on the kagomé lattice, Eur. Phys. J. B **2**, 501 (1998).

[34] Y. Ran, M. Hermele, P. A. Lee, and X.-G. Wen, Projected-Wave-Function Study of the Spin-1/2 Heisenberg Model on the Kagomé Lattice, Phys. Rev. Lett. **98**, 117205 (2007).

[35] R. R. P. Singh and D. A. Huse, Ground state of the spin-1/2 kagome-lattice Heisenberg antiferromagnet, Phys. Rev. B **76**, 180407(R) (2007).

[36] M. Hermele, Y. Ran, P. A. Lee, and X.-G. Wen, Properties of an algebraic spin liquid on the kagome lattice, Phys. Rev. B **77**, 224413 (2008).

[37] S. Yan, D. A. Huse, and S. R. White, Spin-liquid ground state of the $S = 1/2$ kagome Heisenberg antiferromagnet, Science **332**, 1173 (2011).

[38] S. Depenbrock, I. P. McCulloch, and U. Schollwock, Nature of the Spin-Liquid Ground State of the $S = 1/2$ Heisenberg Model on the Kagome Lattice, Phys. Rev. Lett. **109**, 067201 (2012).

[39] B. K. Clark, J. M. Kinder, E. Neuscamman, Garnet Kin-Lic Chan, and M. J. Lawler, Striped Spin Liquid Crystal Ground State Instability of Kagome Antiferromagnets, Phys. Rev. Lett. **111**, 187205 (2013).

[40] Y. Iqbal, F. Becca, S. Sorella, and D. Poilblanc, Gapless spin-liquid phase in the kagome spin-$\frac{1}{2}$ Heisenberg antiferromagnet, Phys. Rev. B **87**, 060405(R) (2013).

[41] Y. Iqbal, D. Poilblanc, and F. Becca, Vanishing spin gap in a competing spin-liquid phase in the kagome Heisenberg antiferromagnet, Phys. Rev. B **89**, 020407(R) (2014).

[42] Y.-C. He, M. P. Zaletel, M. Oshikawa, and F. Pollmann, Signatures of Dirac Cones in a DMRG Study of the Kagome Heisenberg Model, Phys. Rev. X **7**, 031020 (2017).

[43] H. J. Liao, Z. Y. Xie, J. Chen, Z. Y. Liu, H. D. Xie, R. Z. Huang, B. Normand, and T. Xiang, Gapless Spin-Liquid Ground State in the $S = 1/2$ Kagome Antiferromagnet, Phys. Rev. Lett. **118**, 137202 (2017).

[44] X. Chen, S.-J. Ran, T. Liu, C. Peng, Y.-Z. Huang, and G. Su, Thermodynamics of spin-1/2 kagomé Heisenberg antiferromagnet: Algebraic paramagnetic liquid and finite-temperature phase diagram, Sci. Bulletin **63**, 1545 (2018).

[45] C. Hotta and K. Asano, Magnetic susceptibility of quantum spin systems calculated by sine square deformation: One-dimensional, square lattice, and kagome lattice Heisenberg antiferromagnets, Phys. Rev. B **98**, 140405(R) (2018).

[46] C.-Y. Lee, B. Normand, and Y.-J. Kao, Gapless spin liquid in the kagome Heisenberg antiferromagnet with Dzyaloshinskii-Moriya interactions, Phys. Rev. B **98**, 224414 (2018).

[47] W. Zhu, X. Chen, Y.-C. He, and W. Witczak-Krempa, Entanglement signatures of emergent dirac fermions: Kagome spin liquid and quantum criticality, Sci. Adv. **4**, eaat553 (2018).

[48] M. Hering, J. Sonnenschein, Y. Iqbal, and J. Reuther, Characterization of quantum spin liquids and their spinon band structures via functional renormalization, Phys. Rev. B **99**, 100405(R) (2019).

[49] S. Jiang, P. Kim, J. H. Han, and Y. Ran, Competing spin liquid phases in the $S = \frac{1}{2}$ Heisenberg model on the kagome lattice, SciPost Phys. **7**, 006 (2019).

[50] A. M. Lauchli, J. Sudan, and R. Moessner, $S = \frac{1}{2}$ kagome Heisenberg antiferromagnet revisited, Phys. Rev. B **100**, 155142 (2019).

[51] C. Zhang and T. Li, Variational study of the ground state and spin dynamics of the spin-$\frac{1}{2}$ kagome antiferromagnetic Heisenberg model and its implication for herbertsmithite $ZnCu_3(OH)_6Cl_2$, Phys. Rev. B **102**, 195106 (2020).

[52] O. I. Motrunich, Variational study of triangular lattice spin-1/2 model with ring exchanges and spin liquid state in κ-$(ET)_2$ $Cu_2(CN)_3$, Phys. Rev. B **72**, 045105 (2005).

[53] J. S. Helton, K. Matan, M. P. Shores, E. A. Nytko, B. M. Bartlett, Y. Yoshida, Y. Takano, A. Suslov, Y. Qiu, J.-H. Chung, D. G. Nocera, and Y. S. Lee, Spin Dynamics of the Spin-1/2 Kagome Lattice Antiferromagnet $ZnCu_3(OH)_6Cl_2$, Phys. Rev. Lett. **98**, 107204 (2007).

[54] M. A. de Vries, K. V. Kamenev, W. A. Kockelmann, J. Sanchez-Benitez, and A. Harrison, Magnetic Ground State of an Experimental $S = 1/2$ Kagome Antiferromagnet, Phys. Rev. Lett. **100**, 157205 (2008).

[55] T.-H. Han, R. Chisnell, C. J. Bonnoit, D. E. Freedman, V. S. Zapf, N. Harrison, D. G. Nocera, Y. Takano, and Y. S. Lee, Thermodynamic properties of the quantum spin liquid candidate $ZnCu_3(OH)_6Cl_2$ in high magnetic fields, arXiv:1402.2693.

[56] A. Olariu, P. Mendels, F. Bert, F. Duc, J. C. Trombe, M. A. de Vries, and A. Harrison, ^{17}O NMR Study of the Intrinsic Magnetic Susceptibility and Spin Dynamics of the Quantum Kagome Antiferromagnet $ZnCu_3(OH)_6Cl_2$, Phys. Rev. Lett. **100**, 087202 (2008).

[57] J. Wang, W. Yuan, P. M. Singer, R. W. Smaha, W. He, J. Wen, Y. S. Lee, and T. Imai, Emergence of spin singlets with inhomogeneous gaps in the kagome lattice Heisenberg antiferromagnets Zn-barlowite and herbertsmithite, Nat. Phys. **17**, 1109 (2021).

[58] P. Mendels *et al.* (unpublished).

[59] M. Jeong, F. Bert, P. Mendels, F. Duc, J. C. Trombe, M. A. de Vries, and A. Harrison, Field-Induced Freezing of a Quantum Spin Liquid on the Kagome Lattice, Phys. Rev. Lett. **107**, 237201 (2011).

[60] M. Gomilšek, M. Klanjšek, R. Zitko, M. Pregelj, F. Bert, P. Mendels, Y. Li, Q. M. Zhang, and A. Zorko, Field-Induced Instability of a Gapless Spin Liquid with a Spinon Fermi Surface, Phys. Rev. Lett. **119**, 137205 (2017).

[61] T. Asaba, T.-H. Han, B. J. Lawson, F. Yu, C. Tinsman, Z. Xiang, G. Li, Y. S. Lee, and L. Li, High-field magnetic ground state in $S = \frac{1}{2}$ kagome lattice antiferromagnet $ZnCu_3(OH)_6Cl_2$, Phys. Rev. B **90**, 064417 (2014).

[62] J. S. Helton, The ground state of the spin-1/2 kagomé lattice antiferromagnet: Neutron scattering studies of the zinc-paratacamite mineral family, Ph.D. thesis, Massachussetts Institute of Technology, 2009.

[63] Y. Y. Huang, Y. Xu, L. Wang, C. C. Zhao, C. P. Tu, J. M. Ni, L. S. Wang, B. L. Pan, Y. Fu, Z. Hao, C. Liu, J.-W. Mei, and S. Y. Li, Heat Transport in Herbertsmithite: Can a Quantum Spin Liquid Survive Disorder? Phys. Rev. Lett. **127**, 267202 (2021).

[64] H. Murayama, T. Tominaga, T. Asaba, A. de Oliveira Silva, Y. Sato, H. Suzuki, Y. Ukai, S. Suetsugu, Y. Kasahara, R.

Okuma, I. Kimchi, and Y. Matsuda, Universal scaling of the specific heat in $S = 1/2$ quantum kagome antiferromagnet herbertsmithite, arXiv:2106.07223.

[65] T.-H. Han, J. S. Helton, S. Chu, A. Prodi, D. K. Singh, C. Mazzoli, P. Müller, D. G. Nocera, and Y. S. Lee, Synthesis and characterization of single crystals of the spin-$\frac{1}{2}$ kagome-lattice antiferromagnets $Zn_xCu_{4-x}(OH)_6Cl_2$, Phys. Rev. B **83**, 100402(R) (2011).

[66] M. Velázquez, F. Bert, P. Mendels, D. Denux, P. Veber, M. Lahaye, and C. Labrugére, Aqueous solution growth at $200\,°C$ and characterizations of pure, ^{17}O-or D-based herbertsmithite $Zn_xCu_{4-x}(OH)_6Cl_2$ single crystals, J. Cryst. Growth **531**, 125372 (2020).

[67] Y. Werman, S. Chatterjee, S. C. Morampudi, and E. Berg, Signatures of Fractionalization in Spin Liquids from Interlayer Thermal Transport, Phys. Rev. X **8**, 031064 (2018).

[68] L. Chen, M.-E. Boulanger, Z.-C. Wang, F. Tafti, and L. Taillefer, Large phonon thermal hall conductivity in the antiferromagnetic insulator Cu_3TeO_6, Proc. Natl. Acad. Sci. USA **119**, e2208016119 (2022).

[69] H. Alloul, J. Bobroff, M. Gabay, and P. J. Hirschfeld, Defects in correlated metals and superconductors, Rev. Mod. Phys. **81**, 45 (2009).

[70] M. F. Smith, J. Paglione, M. B. Walker, and L. Taillefer, Origin of anomalous low-temperature downturns in the thermal conductivity of cuprates, Phys. Rev. B **71**, 014506 (2005).

[71] H. Katsura, N. Nagaosa, and P. A. Lee, Theory of the Thermal Hall Effect in Quantum Magnets, Phys. Rev. Lett. **104**, 066403 (2010).

[72] J. Callaway, Model for lattice thermal conductivity at low temperatures, Phys. Rev. **113**, 1046 (1959).

[73] G. A. Slack and S. Galginaitis, Thermal conductivity and phonon scattering by magnetic impurities in CdTe, Phys. Rev. **133**, A253 (1964).

[74] B. Fauqué, X. Xu, A. F. Bangura, E. C. Hunter, A. Yamamoto, K. Behnia, A. Carrington, H. Takagi, N. E. Hussey, and R. S. Perry, Thermal conductivity across the metal-insulator transition in the single-crystalline hyperkagome antiferromagnet $Na_{3+x}Ir_3O_8$, Phys. Rev. B **91**, 075129 (2015).

[75] Y. Xu, J. Zhang, Y. S. Li, Y. J. Yu, X. C. Hong, Q. M. Zhang, and S. Y. Li, Absence of Magnetic Thermal Conductivity in the Quantum Spin-Liquid Candidate YbMgGaO$_4$, Phys. Rev. Lett. **117**, 267202 (2016).

[76] Y. J. Yu, Y. Xu, K. J. Ran, J. M. Ni, Y. Y. Huang, J. H. Wang, J. S. Wen, and S. Y. Li, Ultralow-Temperature Thermal Conductivity of the Kitaev Honeycomb Magnet α-RuCl$_3$ Across the Field-Induced Phase Transition, Phys. Rev. Lett. **120**, 067202 (2018).

[77] R. Berman, *Thermal Conduction in Solids*, Oxford Studies in Physics (Oxford University Press, Oxford, 1976).

[78] M.-E. Boulanger, F. Laliberté, M. Dion, S. Badoux, N. Doiron-Leyraud, W. A. Phelan, S. M. Koohpayeh, W. T. Fuhrman, J. R. Chamorro, T. M. McQueen, X. F. Wang, Y. Nakajima, T. Metz, J. Paglione, and L. Taillefer, Field-dependent heat transport in the kondo insulator SmB_6: Phonons scattered by magnetic impurities, Phys. Rev. B **97**, 245141 (2018).

[79] Y. Hirokane, Y. Nii, Y. Tomioka, and Y. Onose, Phononic thermal Hall effect in diluted terbium oxides, Phys. Rev. B **99**, 134419 (2019).

[80] C. A. Pocs, I. A. Leahy, H. Zheng, G. Cao, E.-S. Choi, S.-H. Do, K.-Y. Choi, B. Normand, and M. Lee, Giant thermal magnetoconductivity in CrCl$_3$ and a general model for spin-phonon scattering, Phys. Rev. Res. **2**, 013059 (2020).

[81] R. Okuma, D. Nakamura, and S. Takeyama, Magnetization plateau observed by ultrahigh-field faraday rotation in the kagome antiferromagnet herbertsmithite, Phys. Rev. B **102**, 104429 (2020).

[82] A. Zorko, M. Herak, M. Gomilsek, J. van Tol, M. Velazquez, P. Khuntia, F. Bert, and P. Mendels, Symmetry Reduction in the Quantum Kagome Antiferromagnet Herbertsmithite, Phys. Rev. Lett. **118**, 017202 (2017).

[83] F. Bert, S. Nakamae, F. Ladieu, D. L'Hôte, P. Bonville, F. Duc, J.-C. Trombe, and P. Mendels, Low temperature magnetization of the $S = \frac{1}{2}$ kagome antiferromagnet ZnCu$_3$(OH)$_6$Cl$_2$, Phys. Rev. B **76**, 132411 (2007).

[84] S. Florens, L. Fritz, and M. Vojta, Kondo Effect in Bosonic Spin Liquids, Phys. Rev. Lett. **96**, 036601 (2006).

[85] M. Gomilšek, R. Žitko, M. Klanjšek, M. Pregelj, C. Baines, Y. Li, Q. M. Zhang, and A. Zorko, Kondo screening in a charge-insulating spinon metal, Nat. Phys. **15**, 754 (2019).

[86] A. Kolezhuk, S. Sachdev, R. R. Biswas, and P. Chen, Theory of quantum impurities in spin liquids, Phys. Rev. B **74**, 165114 (2006).

[87] K. Gregor and O. I. Motrunich, Nonmagnetic impurities in the spin-1/2 kagome antiferromagnet, Phys. Rev. B **77**, 184423 (2008).

[88] I. Rousochatzakis, S. R. Manmana, A. M. Lauchli, B. Normand, and F. Mila, Dzyaloshinskii-Moriya anisotropy and nonmagnetic impurities in the $s = \frac{1}{2}$ kagome system ZnCu$_3$(OH)$_6$Cl$_2$, Phys. Rev. B **79**, 214415 (2009).

[89] P. Patil, F. Alet, S. Capponi, and K. Damle, Quantum half-orphans in kagome antiferromagnets, Phys. Rev. Res. **2**, 043425 (2020).

[90] R. R. P. Singh, Valence Bond Glass Phase in Dilute Kagome Antiferromagnets, Phys. Rev. Lett. **104**, 177203 (2010).

[91] H. Kawamura, K. Watanabe, and T. Shimokawa, Quantum spin-liquid behavior in the spin-1/2 random-bond Heisenberg antiferromagnet on the kagome lattice, J. Phys. Soc. Jpn. **83**, 103704 (2014).

[92] I. Kimchi, J. P. Sheckelton, T. M. McQueen, and P. A. Lee, Scaling and data collapse from local moments in frustrated disordered quantum spin systems, Nat. Commun. **9**, 4367 (2018).

[93] N. J. Laurita, A. Ron, J. W. Han, A. Scheie, J. P. Sheckelton, R. W. Smaha, W. He, J.-J. Wen, J. S. Lee, Y. S. Lee, M. R. Norman, and D. Hsieh, Evidence for a parity broken monoclinic ground state in the $S = 1/2$ kagomé antiferromagnet herbertsmithite, arXiv:1910.13606.

[94] T. Imai, E. A. Nytko, B. M. Bartlett, M. P. Shores, and D. G. Nocera, ^{63}Cu, ^{35}Cl, and ^1H NMR in the $S = \frac{1}{2}$ Kagome Lattice ZnCu$_3$(OH)$_6$Cl$_2$, Phys. Rev. Lett. **100**, 077203 (2008).

[95] M. Fu, T. Imai, T.-H. Han, and Y. S. Lee, Evidence for a gapped spin-liquid ground state in a kagome Heisenberg antiferromagnet, Science **350**, 655 (2015).

[96] M. Hirschberger, R. Chisnell, Y. S. Lee, and N. P. Ong, Thermal Hall Effect of Spin Excitations in a Kagome Magnet, Phys. Rev. Lett. **115**, 106603 (2015).

[97] Y. Onose, T. Ideue, H. Katsura, Y. Shiomi, N. Nagaosa, and Y. Tokura, Observation of the magnon Hall effect, Science **329**, 297 (2010).

[98] M. Hirschberger, J. W. Krizan, R. J. Cava, and N. P. Ong, Large thermal Hall conductivity of neutral spin excitations in a frustrated quantum magnet, Science **348**, 106 (2015).

[99] T. Yokoi, S. Ma, Y. Kasahara, S. Kasahara, T. Shibauchi, N. Kurita, H. Tanaka, J. Nasu, Y. Motome, C. Hickey, S. Trebst, and Y. Matsuda, Half-integer quantized anomalous thermal Hall effect in the Kitaev material candidate α-RuCl$_3$, Science **373**, 568 (2021).

[100] J. A. N. Bruin, R. R. Claus, Y. Matsumoto, N. Kurita, H. Tanaka, and H. Takagi, Robustness of the thermal Hall effect close to half-quantization in α-RuCl$_3$, Nat. Phys. **18**, 401 (2022).

[101] P. Czajka, T. Gao, M. Hirschberger, P. Lampen-Kelley, A. Banerjee, N. Quirk, D. G. Mandrus, S. E. Nagler, and N. P. Ong, The planar thermal Hall conductivity in the Kitaev magnet α-RuCl$_3$, Nat. Mater. **22**, 36 (2023).

[102] C. Strohm, G. L. J. A. Rikken, and P. Wyder, Phenomenological Evidence for the Phonon Hall Effect, Phys. Rev. Lett. **95**, 155901 (2005).

[103] A. V. Inyushkin and A. N. Taldenkov, On the phonon Hall effect in a paramagnetic dielectric, JETP Lett. **86**, 379 (2007).

[104] T. Ideue, T. Kurumaji, S. Ishiwata, and Y. Tokura, Giant thermal Hall effect in multiferroics, Nat. Mater. **16**, 797 (2017).

[105] G. Grissonnanche, A. Legros, S. Badoux, E. Lefrançois, V. Zatko, M. Lizaire, F. Laliberté, A. Gourgout, J.-S. Zhou, S. Pyon, T. Takayama, H. Takagi, S. Ono, N. Doiron-Leyraud, and L. Taillefer, Giant thermal Hall conductivity in the pseudogap phase of cuprate superconductors, Nature (London) **571**, 376 (2019).

[106] M.-E. Boulanger, G. Grissonnanche, S. Badoux, A. Allaire, E. Lefrançois, A. Legros, A. Gourgout, M. Dion, C. H. Wang, X. H. Chen, R. Liang, W. N. Hardy, D. A. Bonn, and L. Taillefer, Thermal Hall conductivity in the cuprate Mott insulators Nd$_2$CuO$_4$ and Sr$_2$CuO$_2$Cl$_2$, Nat. Commun. **11**, 5325 (2020).

[107] G. Grissonnanche, S. Thériault, A. Gourgout, M.-E. Boulanger, E. Lefrançois, A. Ataei, F. Laliberté, M. Dion, J.-S.

Zhou, S. Pyon, T. Takayama, H. Takagi, N. Doiron-Leyraud, and L. Taillefer, Chiral phonons in the pseudogap phase of cuprates, Nat. Phys. **16**, 1108 (2020).

[108] X. Li, B. Fauqué, Z. Zhu, and K. Behnia, Phonon Thermal Hall Effect in Strontium Titanate, Phys. Rev. Lett. **124**, 105901 (2020).

[109] T. Qin, J. Zhou, and J. Shi, Berry curvature and the phonon Hall effect, Phys. Rev. B **86**, 104305 (2012).

[110] J.-Y. Chen, S. A. Kivelson, and X.-Q. Sun, Enhanced Thermal Hall Effect in Nearly Ferroelectric Insulators, Phys. Rev. Lett. **124**, 167601 (2020).

[111] V. Kocsis, D. A. S. Kaib, K. Riedl, S. Gass, P. Lampen-Kelley, D. G. Mandrus, S. E. Nagler, N. Pérez, K. Nielsch, B. Büchner, A. U. B. Wolter, and R. Valentí, Magnetoelastic coupling anisotropy in the Kitaev material α-RuCl$_3$, Phys. Rev. B **105**, 094410 (2022).

[112] H. Guo and S. Sachdev, Extrinsic phonon thermal Hall transport from Hall viscosity, Phys. Rev. B **103**, 205115 (2021).

[113] X.-Q. Sun, J.-Y. Chen, and S. A. Kivelson, Large extrinsic phonon thermal Hall effect from resonant scattering, Phys. Rev. B **106**, 144111 (2022).

[114] H. Guo, D. G. Joshi, and S. Sachdev, Resonant thermal Hall effect of phonons coupled to dynamical defects, Proc. Natl. Acad. Sci. USA **119**, e2215141119 (2022).

[115] B. Flebus and A. H. MacDonald, Charged defects and phonon Hall effects in ionic crystals, Phys. Rev. B **105**, L220301 (2022).

[116] M. Mori, A. Spencer-Smith, O. P. Sushkov, and S. Maekawa, Origin of the Phonon Hall Effect in Rare-Earth Garnets, Phys. Rev. Lett. **113**, 265901 (2014).

[117] H. Murayama, T. Tominaga, T. Asaba, A. de Oliveira Silva, Y. Sato, H. Suzuki, Y. Ukai, S. Suetsugu, Y. Kasahara, R. Okuma, I. Kimchi, and Y. Matsuda, Universal scaling of specific heat in the $S = \frac{1}{2}$ quantum kagome antiferromagnet herbertsmithite, Phys. Rev. B **106**, 174406 (2022).